cosmetics

MDPI

Article

Design of Prototype Formulations for In Vitro Dermal Delivery of the Natural Antioxidant Ferulic Acid Based on Ethosomal Colloidal Systems

Cesar A. Londoño [1], John Rojas [1], Cristhian J. Yarce [2] and Constain H. Salamanca [2,*]

[1] Departamento de Farmacia, Facultad de Ciencias Farmacéuticas y Alimentarias, Universidad de Antioquia, Medellín 050010, Colombia; cesarlondonoqf@gmail.com (C.A.L.); jrojasca@gmail.com (J.R.)

[2] Departamento de Ciencias Farmacéuticas, Facultad de Ciencias Naturales, Universidad Icesi, Calle 18 No. 122–135, Cali 76003, Colombia; cjyarce@icesi.edu.co

* Correspondence: chsalamanca@icesi.edu.co; Tel.: +57-2-5552334

Received: 17 November 2018; Accepted: 16 January 2019; Published: 19 January 2019

Abstract: Ferulic acid (FA), a naturally occurring antioxidant, is currently used to prevent skin damage. However, FA is very unstable upon exposure to UV radiation and other factors, which decrease its shelf-life and effectiveness. Therefore, in this work, different prototypes of ethosomal FA vesicular systems were designed and developed to provide protection against different environmental factors. A two-level fractional factorial design was employed using particle size, zeta potential (ZP), incorporation efficiency (EE), polydispersity index (PDI), and the existing relationship between length and width of vesicles or aspect ratio (AR) as response variables. The optimal formulation was characterized using differential scanning calorimetry (DSC), infrared analysis, UV-Vis absorption, in-vitro permeability, and thermal degradation studies. Depending on the processing conditions, the EE and particle size varied between 3 and 87% and 470 and 1208 nm, respectively. Membrane studies indicated that the free product released ~4.8% of the compound, whereas the encapsulated material released ~7.1%. Because of their enhanced permeability, ethosomes could be a promising alternative for the topical administration of antioxidants to reduce the oxidative damage caused by solar radiation.

Keywords: ethosomes; ferulic acid; antioxidant; dermal diffusion; chemical stabilization

1. Introduction

Skin damage caused by sun exposure is the most prevalent dermatological problem in the world. Currently, two to three million cases of non-melanoma skin cancer, and 132000 cases of melanomas are diagnosed each year. Moreover, one of every three types of cancer corresponds to skin cancer [1]. UVA radiation can penetrate the dermis and generate reactive oxygen species [2]. In turn, those could trigger lipid peroxidation of the cell membrane, therefore causing melanomas, dermatitis, premature aging, inflammation, and other types of severe skin problems [3]. Many organic compounds are currently used to prevent skin damage caused by solar radiation. However, these compounds are mostly unstable, and solar radiation decreases their shelf-life and effectiveness. To address this concern, several natural antioxidants of the phenolic compound family are currently incorporated into those products. These antioxidants are present in a large variety of plants, fruits, and vegetables [4]. Ferulic acid (FA) is one of the most remarkable phenolic compounds due to its functional versatility. FA is part of the cinnamate family and is present in plants such as corn, rice, peanuts, tomatoes, coffee, and wheat, where it plays an essential role in preservation, reinforcing the plant cell wall, and offering protection against microbial and solar damage [5]. FA is a weak acid with hydrophobic characteristics

and has a maximum absorption wavelength of 321 nm [6]. FA is also considered a good whitener that presents anti-aging, anti-diabetic, anti-inflammatory, and anti-cancer properties. FA can effectively treat dermatological conditions such as rosacea, and presents neuroprotective and cardioprotective properties [3]. Unfortunately, FA is unstable if stored at high temperatures and extreme pH levels and undergoes isomerization and degradation reactions that alter the color and odor of the finished products. Furthermore, photodegradation by exposure to sunlight also decreases its safety and efficacy and generates oxidation products such as quinines, dimers, and aldehydes [4].

Nowadays, ethosomal micro incorporation is a feasible alternative to improve the stability and skin permeability of FA. Ethosomes are flexible vesicles formed using phospholipids, water, and high amounts of ethanol (20–45%), which confers some degree of steric stabilization by preventing agglomeration and loss of functional activity [7]. Ethanol also improves membrane permeability and interacts with the polar heads of lipid molecules, thus decreasing the phase transition temperature of the lipids located in the stratum corneum of the skin. Therefore, these vesicles increase the fluidity of the lipid molecules and improve the permeability of cell membranes. Thus, compared to conventional liposomes and nanoparticles, they are more efficient when releasing high-and low-molecular weight lipophilic and hydrophilic compounds regarding to the loading and penetration [8,9]. In addition, ethosomes are a convenient and cost-effective alternative that overcome the hassle of large-scale liposome manufacturing using conventional methods, its composition is safe, and the components are approved for pharmaceutical and cosmetic use and do not require any sophisticated or specially designed equipment [7,10].

The ethosomal phospholipids resemble those of cell membranes, and exhibit phase transitions. At the phase transition temperature, the membrane is transformed from a fully extended and closely packed "gel phase" to a liquid crystalline disordered "fluid phase" [11]. Thus, when a mixture of phospholipids is hydrated using excess water, at least two different lamellar phases are formed. The first one, the gel phase, occurs at lower temperatures and is characterized by molecules packed in a quasi-crystalline two-dimensional lattice [12]. The second one, the lamellar phase, is a fluid liquid-crystalline phase where lipid molecules can rapidly diffuse into the plane of the lipid bilayer. The largest permeability occurs in the vicinity of this phase transition [13]. Scientists have been employing ethosomes for the dermal release of cannabidiol while preventing its side effects and improving its dermis and muscle tissue penetration. Furthermore, these ethosomes presented enhanced anti-inflammatory and anti-edema effects in mice [14]. In another study, chitosan vesicles that were prepared by ionic gelation using FA inhibited the metabolic activity of *C. albicans* to 22.5% after 24 h of incubation [15]. Encapsulating FA using ethosomes could increase its stability and skin penetration. The goal of this study was to increase the shelf-life and dermal diffusion of FA using ethosomal microcarriers.

2. Experiment

2.1. Materials

Ferulic acid (lot BCBQ6979V) was obtained from Sigma Aldrich (St. Louis, MO, USA), ethanol (lot k46867483533) was purchased from Merck (Kenilworth, NJ, USA), and triethanolamine (lot 5MO14651) and polyethylene glycol 400 (lot 875967) were purchased from PanReac (Barcelona, Spain). Deionized water was used as medium for preparing ethosomes. Propylene glycol USP (lot 102025-1) and soy lecithin (lot 1212035-2) were received from Quimicos JM SA (Medellin, Colombia). All materials were of analytical grade.

2.2. Methods

2.2.1. Experimental Design, Statistical Analysis, and Process Optimization

A two-level full factorial experimental design was conducted for the products obtained using the described processing methods. Each process consisted of eight experimental runs where the FA load (FAL) (i.e., 10 and 100 mg or 0.01 and 0.1 % w/v, respectively), homogenization time (HT) (i.e., 5 and 15 min) and homogenization rate (HR) (i.e., 3000 and 151,000 rpm) were the processing variables (Table 1). The particle size, zeta potential (ZP), entrapment efficiency (EE), and aspect ratio (AR) of the vesicles were considered to be dependent variables. The Design Expert® software (version 8.04, Stat-Ease, Inc, Minneapolis, MN, USA) was used for data analysis. Analysis of variance with a 95% confidence level was also conducted. In addition, the accuracy and validity of the model to represent the experimental data were assessed and the level of significance of each term of the adjusted model (*p*-value), coefficient of determination (r^2), and lack of adjustment were considered. Matching the response variables to the results was based on the following selected multiple regression model: $y = b_1x_1 + b_2x_2 + b_3x_3 + b_{12}x_1x_2 + b_{13}x_1x_3 + b_{23}x_2x_3$. The model used a "backward elimination" option, where y is the approximate value of the output quantity, b_1, b_2, and b_3 are predictors of the regression coefficients, and x_1, x_2, and x_3 are the approximate values of the input quantities. The best set of processing conditions was selected from the response grid search and desirability function to obtain a system with the lowest polydispersity index (PDI), and highest ZP, EE, and AR [16,17].

2.2.2. Production of Ethosomal Systems

Hot Processing Method

Ethosomes were prepared using FA (10 and 100 mg), soy lecithin (3%), ethanol (30%), propylene glycol (20%) and deionized water (q.s). First, FA was dissolved in a mixture of ethanol and propylene glycol, which was then added to the lecithin phase dispersed in water at 40 °C to prevent the solidification of the lipid phase. Subsequently, the hydro-alcoholic dispersion was stirred for 5 min and sonicated at 4 °C for three cycles, a resting time of 5 min being used between cycles [18]. Afterward, the ethosomal system was homogenized using 5 min cycles utilizing an ULTRA-TURRAX homogenizer (IKA UltraTurrax T18BS1, Ika-Werke, Staufen im Breisgau, Germany) at 40 °C.

Cold Processing Method

The same proportions of components used for the hot processing method were employed for the cold processing method. Briefly, soy lecithin and FA were dissolved in ethanol under vigorous magnetic stirring at 25 °C. Subsequently, propylene glycol was added to the solution, which was previously heated at 30 °C. This mixture was then added to another vessel that contained deionized water at 30 °C and stirred for 5 min. Finally, the samples were sonicated, homogenized, and cooled down to 4 °C [11].

2.2.3. Morphology and Surface Analysis of the Vesicles

The morphology and structure of the dispersed ethosomes were analyzed using a scanning electron microscopy (SEM) (JEOL 6490LV, Peabody, MA, USA). Approximately, 0.2 mL dispersions were spread evenly on an aluminum stub and sputter-coated using a vacuum chamber (Desk IV, Denton Vacuum, Moorestown, NJ, USA) with a 30% gold coating for 5 min; the chamber was operated at 12 kV. Approximately, 650 particles from the SEM images were processed using the ImageJ® software (version 1.46r, NIH, Bethesda, MD, USA) to obtain the average AR, which was used as the main shape descriptor.

2.2.4. Dynamic Light Scattering (DLS) Characterization

A Malvern Nano-ZS90 Zetasizer using the laser Doppler velocimetry principle and coupled with a Zetasizer software (vs. 7.11, Malvern Instruments Ltd., Malvern, UK) was employed at 25 °C. After purging the system, the small volume cell was filled with 2 mL distilled water. Subsequently, 150 µL of sample was added to the cell to achieve a 12–13% darkening of the laser beam to obtain particle size readings within the measuring range. The ZP measurements were performed by adding 700 µL of sample to a polystyrene cell and adjusting the temperature to 25 °C. Samples were analyzed for 12 to 16 cycles at the voltage of 4 mV. Light scattering measurements were performed at least in triplicate. On the other hand, the PDI was determined using DLS at the wavelength of 677 nm using a 15-mW solid-state laser as light source. The scattered light was detected at the dispersion angle of 173° (backscatter) and 13° (Forward scatter), with this information, the software can calculate a dispersion ratio between large and small particles. It is important to notice that in light scattering, the term polydispersity is coming from a cumulant analysis of the DLS of the autocorrelation function. In the cumulant analysis, a single particle size mode is assumed, and a single exponential fit is applied to an autocorrelation function defined for the movement of a particle in the media and the polydispersity describes the width of the assumed Gaussian distribution.

2.2.5. EE Measurements

10 mL aliquots of each sample were centrifuged using a Micro-Semi Centricone 10-T-5 instrument (Precision Scientific, Chicago, IL, USA) at 1550 rpm for 1.5 h. The supernatant was diluted 100 and 40 times using a mixture of water, ethanol, and propylene glycol (50:30:20 % v/v) as dispersion medium, and the FAL was 100 and 10 mg. The absorbance of the resulting samples were measured using a UV-Vis spectrophotometer (HACH DR 5000, Hach Company, Loveland, Colorado) at the wavelength of 321 nm, and the amount of FA was determined by interpolation from a calibration curve built at the concentrations of 1, 2, 5, 10 and 12 µg/mL. The amount of encapsulated FA was calculated using the following equation:

$$EE = \left(\frac{Q_t - Q_s}{Q_t} \right) \times 100\% \quad (1)$$

where Q_t is the total amount of FA and Q_s is the amount of free FA in the supernatant after centrifugation.

2.2.6. Characterization of Optimized Ethosomal Systems Using Fourier-Transform Infrared (FT-IR) Spectroscopy and Differential Scanning Calorimetry (DSC)

The infrared spectra of the compounds were obtained on an FT-IR spectrophotometer (Thermo Nicolet 6700, Fisher Scientific, Waltham, Massachusetts, USA), and the data were analyzed using the Origin® software. Approximately, 2 mg of sample was ground along with KBr (~200 mg) using a mortar and pestle and was subsequently compressed at 150 MPa for 5 min in a hydraulic press. The spectra were measured between 4000 and 400 cm^{-1} employing 16 scans at a resolution of 2 cm^{-1}. The thermal behavior of the lipid vesicles was evaluated using a DSC device (Q2000, TA Instruments, New Castle, DE, USA) and calibrated with indium at a modulated temperature. Approximately, 20 mg of sample was placed in a sealed aluminum crucible under a constant stream of nitrogen (30 mL/min). An empty sealed aluminum crucible was used as reference. Thermograms were collected between 25 and 450 °C at the heating rate of 10 °C/min.

2.2.7. Physical Stability of Optimized Ethosomal Systems Analyzed Using DLS

The effect of the pH of the medium on the ZP and size of the vesicles was analyzed using a Zetasizer (Nano ZSP, Malvern Instrument, WORCS, UK) equipped with an automatic titrator and a disposable folded capillary cell (DTS1070) at 25 °C. All measurements were performed in triplicate.

2.2.8. Performance Tests

In-Vitro Permeability Test

The ability of the free and encapsulated FA to diffuse through membranes was determined using Franz cells equipped with different synthetic cellulose ester membranes featuring 0.45 µm pores (EMD Millipore) and wetted for 0.5 h in a petri dish with soy lecithin. These results were compared with those obtained using the Strat-M® membranes (Sigma-Aldrich), which are synthetic membranes designed to simulate human skin [19]. These synthetic membranes are used to study the diffusion rate of bioactive compounds, and consist of three stratified layers of polyolefin, polyethersulfone, and synthetic lipids. The first polyolefin layer presents large pores and is highly diffusive, whereas the polyethersulfone inner layer exhibits smaller pores, and hence, presents a greater diffusion resistance [20]. Each membrane was carefully inserted between the two compartments of a Franz cell. The receptor compartment (13.0 mL capacity) was filled with two different media: (i) solution A which consisted of water, ethanol, and propylene glycol (50:30:20 % v/v), and (ii) solution B which consisted of ethanol, propylene glycol, and phosphate buffer (pH 7.4) at a 30:20:50 % v/v. Subsequently, 3.0 mL of free solution (solution A with a concentration of 1 mg/mL) or encapsulated FA solution (1 mg/mL) was added to the donor compartment. The assays were performed at the membrane temperature of 32 ± 1 °C and at 240 rpm for 6 h, and 1.0 mL aliquots were collected every hour. Each aliquot was replaced with an equal volume of the medium employed. The amount of FA was measured by UV spectrophotometry at the maximum wavelength of 321 nm. The flux (J) was determined from the slope of the linear section of the diffusion profile (mg/cm^2·h). The amount of FA released was fitted to the following solution of Fick's second law of diffusion:

$$C = C_0 \times erfc\left(\frac{x}{2\left(\sqrt{D \times t}\right)}\right) \quad (2)$$

where, C is the concentration of FA (mg/mL), C_0 is the initial concentration of FA in the donor compartment, $erfc$ is the complementary error function, x is the diffusion distance (1 cm), and D is the fitted diffusion coefficient.

3. Results and Discussion

3.1. Effect of Processing Conditions on Physical Properties of Vesicles

To form ethosomal systems, energy should be transferred to the substances used to generate the vesicles. In this study, energy was supplied as heat, followed by agitation, sonication, and homogenization. This caused lipid molecules to rearrange and form vesicles which reached thermodynamic equilibrium in aqueous phase. Applying a mechanical force facilitated the homogeneous distribution of the components [21]. During the manufacturing process, water was the main wetting agent for the phospholipids, and an ethanol solution containing FA was added to the vessel. Thus, water and ethanol led to the hydration of the outer phospholipid monolayer and increased the surface of the polar heads, resulting in the formation of multilamellar vesicles. The 40 °C temperature, which was higher than the phase transition temperature of soy lecithin, allowed for the transition of the bilayers from a gel phase (well ordered) to a disordered fluid phase [22]. As a result, as water penetrated them, the hydrocarbon chains were transitioned into a fluid state, leading to melting of the hydrocarbon chain region and dissociating the ionic structure. Once samples were cooled below the phase transition temperature, the hydrocarbon chains rearranged themselves into an orderly crystalline lattice or a quasi-crystalline gel phase [23]. As a result, the thickness of the bilayer decreased and the surface area per molecule increased [17,24]. In addition, there was no risk of lipid degradation since only short homogenization cycles (~5 min) were implemented and the settling time was 5 min. Propylene glycol is a water-soluble and physiologically acceptable compound that

could increase the stability of lipid vesicles. Moreover, the presence of propylene glycol and ethanol led to the formation of flexible ethosomes. The HT was limited to a maximum of 15 min to avoid FA leakage from the vesicles and phospholipid decomposition because of induced heating (~40 °C). The particle size of the vesicles varied depending on the experimental conditions. Some authors indicated that homogenization *per se* produced 400–3500 nm particles, whereas sonication only formed 170–260 nm vesicles. Furthermore, some studies suggested that ethosomes are essentially oligolamellar, multilamellar, and large multilamellar vesicles (OLV, MLV, and LUV, respectively). The latter usually range in size from 500 to 1000 nm. Moreover, MLV present several bilayers that trap the solvent in their core part, and their size is greater than 500 nm. In addition, MLVs from 100 nm to 1 µm in size are also called OLVs [25]. As can be seen in Figure 1, the ethosomal systems obtained in this study belonged to the MLV, OLV, and LUV types, and the vesicle type depended on the processing conditions.

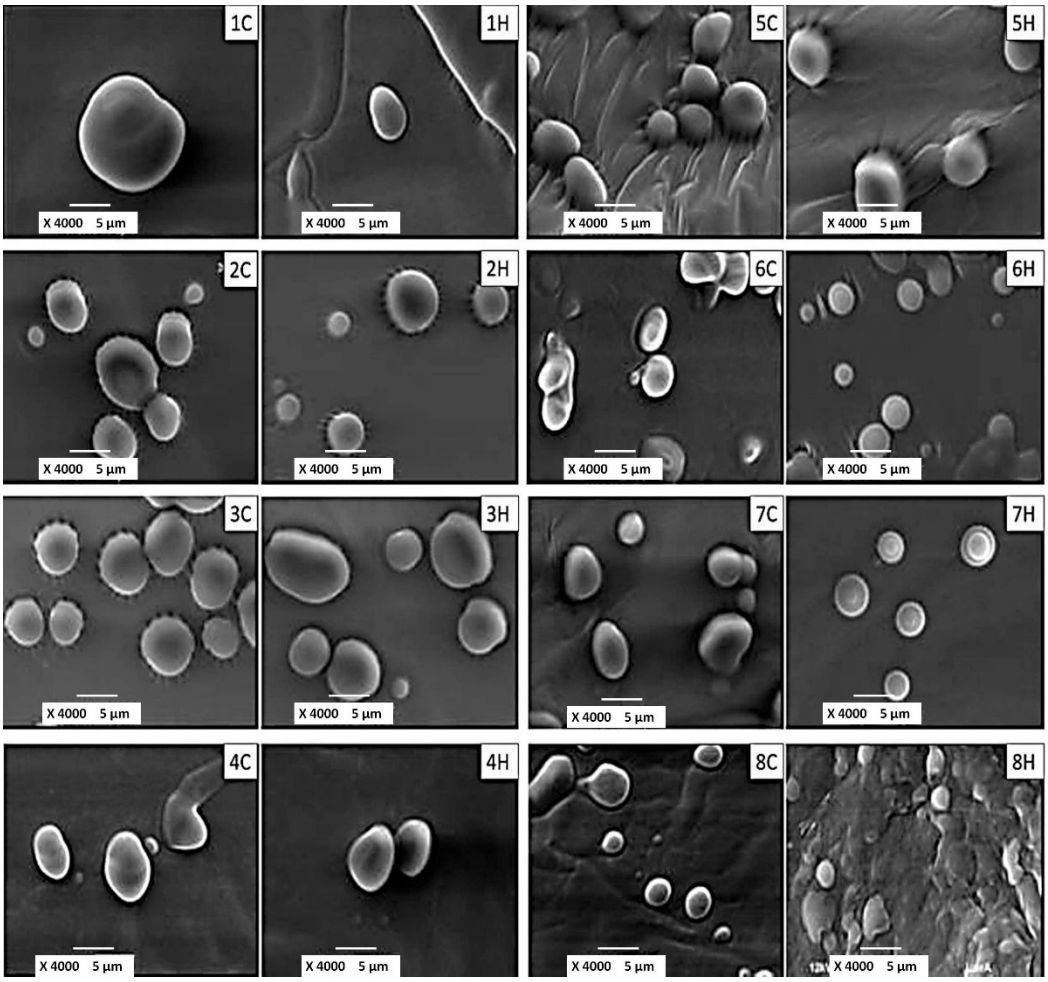

Figure 1. Scanning Electron Microphotographs of ethosomal systems produced under different processing conditions.

The ethosomes exhibited regular and smooth surfaces, and in few cases (i.e., samples 6H and 7H) halos were observed around the vesicles, which were possibly attributed to the prevalence of LUV. These features were independent of the processing conditions. The SEM images of the aqueous dispersions indicated that sample 7H presented the largest number of regular vesicles featuring thick walls. Once these vesicles were subjected to drying, they coalesced and formed a thin film for subsequent analysis by SEM, it is possible that one of the components of the formulation acts as a protector against dehydration, avoiding the tendency of the vesicles to aggregate.

3.2. DLS Characterization of Vesicles

The particle size distribution was determined using DLS, which provided cumulative average size information for many vesicles simultaneously. The information thus obtained agreed with the SEM morphology analysis data. Furthermore, light scattering assumed any aggregates of more than one vesicle to be single particles. Comparable average sizes were obtained from both light scattering and microscopy analyses. Bimodal distributions where obtained for ethosomal systems such as those labeled as 1H, 2H, 5H, and 7H which presented trivial subpopulations between 6 and 9 μm in size. In addition, only the samples labeled as 3H and 4H presented narrow size distributions and exhibited a low FAL (10 mg) and long HT (15 min).

The ZP values refer to the charges on the slipping plane at the surface of the vesicle, and although they are not direct measurements of the surface charge, they are still good estimates. It is well known, that the oppositely charged ions in the slipping plane travel alongside the charged surface, the ions underneath the plane remain attached to the surface. Thus, the ZP values are good indicators of the electrostatic interactions between vesicles and are normally used to predict the stability of dispersions, since colloidal systems are not stable close to the point of zero charge [26]. Even though soy lecithin consists of a mixture of several phospholipids of different charges, phosphatidylcholine (PC) is the most prevalent phospholipid and presents a net charge of zero [27]. Only phosphatidylserine which is present in a lower amount in lecithin features a negative charge rendering a slightly negative charge to the vesicles (−67.7 mV). This negative charge is boosted by the presence of a large fraction of ionized FA. Negatively charged ethosomes exhibit advantages over cationic systems such as stearylamine, which have been reported to be toxic due to the interaction of the cationic lipids with cell organelle membranes. In addition, negatively charged ethosomes are more efficiently associated [26]. Moreover, the net negative charges of the ethosomes increase their physical stability, thus preventing their fusion and aggregation due to electrostatic repulsions. Interestingly, ethanol also renders some degree of steric stabilization to the ethosomes and prevents the aggregation of the vesicles due to electrostatic repulsions [27]. It is expected that FA would be primarily entrapped within the inner aqueous core of ethosomes, where the rigid aromatic ring is oriented between the lipid bilayers near the phosphate head group. Furthermore, phosphate groups could be exposed at the surface of the carboxyl groups of FA, thus providing additional shielding. The magnitude of this protective effect was more noticeable at high FALs. Higher FALs (100 mg) also was prompted to reduce the charge intensity. The results of the different tests performed are listed in the Table 1, and the plots obtained from the factorial models along with the significant factors are depicted in Figure 2.

Table 1. Physicochemical properties of ethosomes obtained using different processing conditions.

Processing Method	Sample ID	FAL (mg)	HT (min)	HR (rpm)	ZP ± SD (mV)	Size ± SD (nm)	PDI ± SD	EE ± SD (%)	AR ± SD
hot	1H	10	5	3000	−86.8 ± 1.5	470.5 ± 6.1	0.59 ± 0.13	3.0 ± 0.05	0.7 ± 0.11
hot	2H	10	5	15,000	−60.9 ± 1.4	566.8 ± 39.8	0.54 ± 0.03	100 ± 0.02	0.7 ± 0.13
hot	3H	10	15	3000	−62.8 ± 0.3	590.5 ± 1353	0.23 ± 0.02	67.0 ± 0.12	0.7 ± 0.14
hot	4H	10	15	15,000	−72.0 ± 0.2	552.0 ± 2.4	0.20 ± 0.02	87.4 ± 0.09	0.8 ± 0.10
hot	5H	100	5	3000	−50.4 ± 2.4	1035 ± 21.9	0.58 ± 0.28	10.6 ± 0.12	0.8 ± 0.12
hot	6H	100	5	15,000	−55.5 ± 1.0	1208 ± 94.8	0.20 ± 0.14	22.2 ± 0.12	0.7 ± 0.14
hot	7H	100	15	3000	−54.3 ± 0.6	1119 ± 87.4	0.44 ± 0.17	49.0 ± 0.06	0.8 ± 0.12
hot	8H	100	15	15,000	−54.9 ± 0.8	929.8 ± 25.1	0.52 ± 0.16	6.2 ± 0.01	0.7 ± 0.10
cold	1C	10	5	3000	−84.8 ± 1.5	885.3 ± 89.3	0.51 ± 0.35	79.6 ± 0.13	0.8 ± 0.14
cold	2C	10	5	15,000	−71.4 ± 0.5	561.0 ± 15.75	0.21 ± 0.14	91.4 ± 0.01	0.7 ± 0.11
cold	3C	10	15	3000	−63.7 ± 1.0	501.5 ± 16.41	0.52 ± 0.04	17.9 ± 0.05	0.7 ± 0.16
cold	4C	10	15	15,000	−72.1 ± 0.9	445.3 ± 9.2	0.39 ± 0.08	100 ± 0.01	0.8 ± 0.09
cold	5C	100	5	3000	−46.3 ± 0.7	579.3 ± 9.7	0.42 ± 0.12	8.4 ± 0.09	0.7 ± 0.18
cold	6C	100	5	15,000	−52.2 ± 0.9	612.7 ± 11.8	0.31 ± 0.11	6.3 ± 0.01	0.7 ± 0.13
cold	7C	100	15	3000	−62.9 ± 0.7	653.4 ± 9.2	0.53 ± 0.09	5.5 ± 0.01	0.7 ± 0.12
cold	8C	100	15	15,000	−54.6 ± 1.3	778.6 ± 31.6	0.26 ± 0.22	0 ± 0.00	0.7 ± 0.14

FAL: ferulic acid load, HT: homogenization time, HR: homogenization rate, PDI: polydispersity index, ZP: zeta potential, EE: encapsulation efficiency, AR: aspect ratio. The standard deviation was obtained by replicates in triplicate.

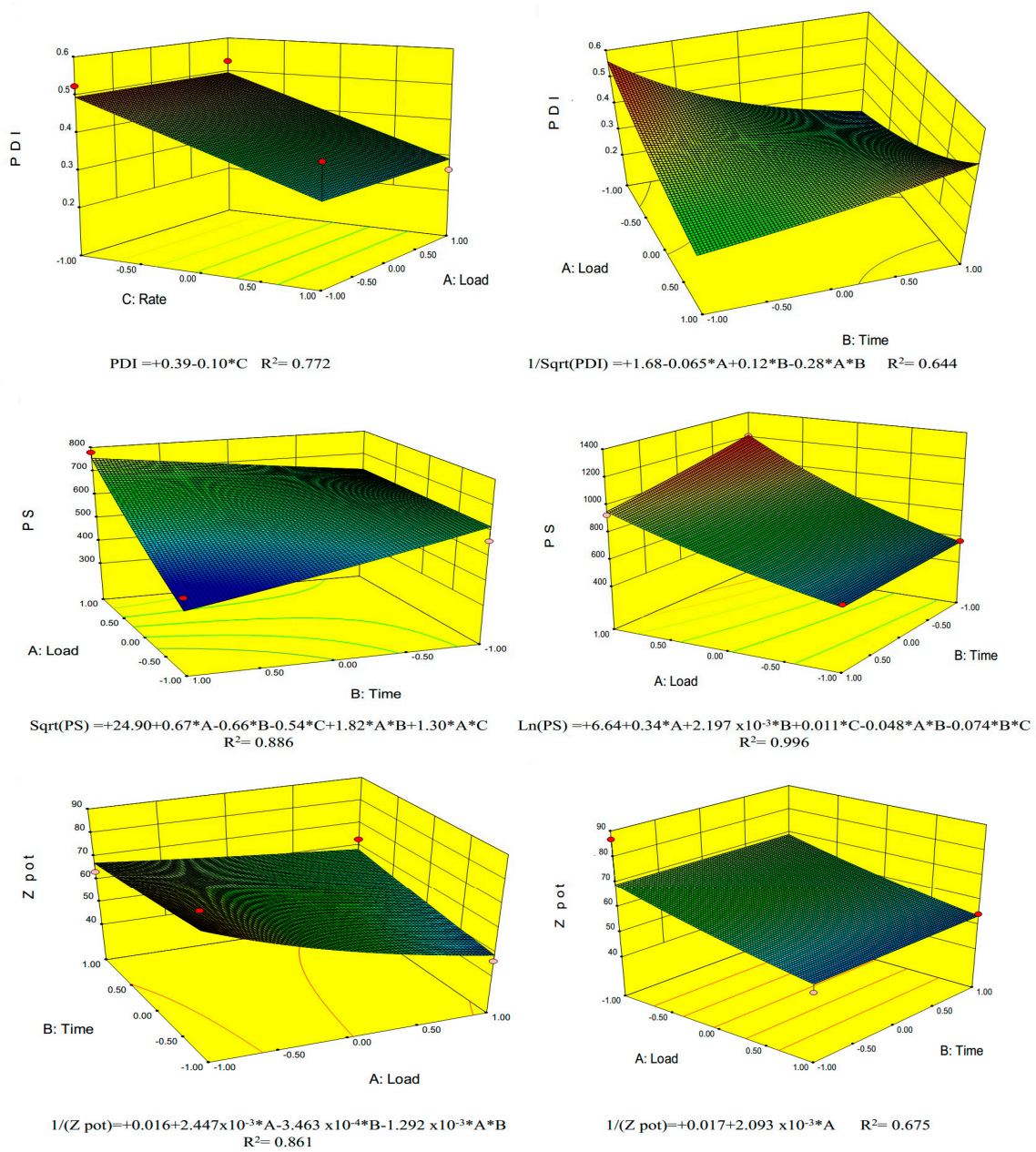

(**A**)

Figure 2. *Cont.*

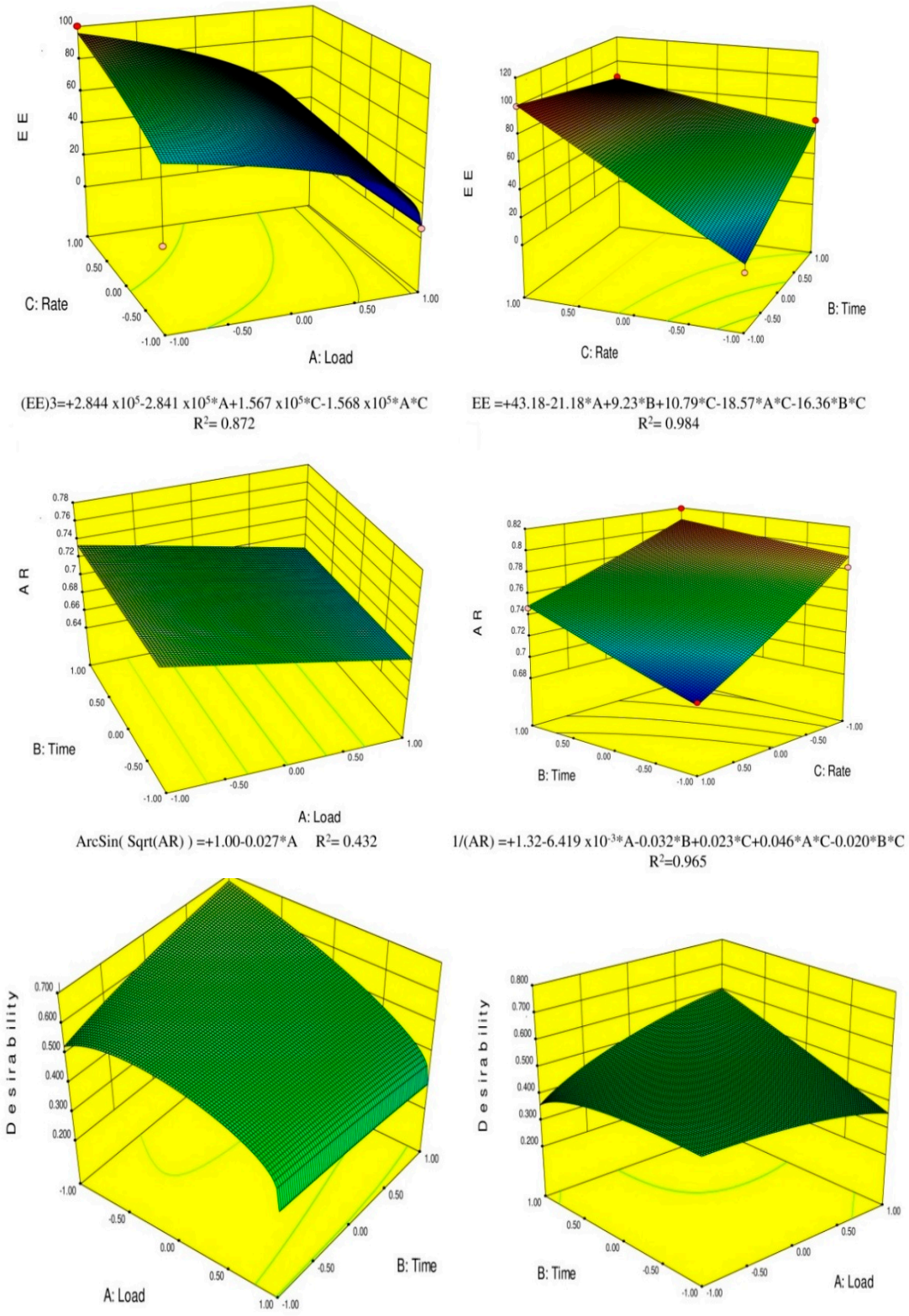

(**B**)

Figure 2. (**A**) Response surface graphics for preparation methods in cold (**Left**) and hot (**Right**) for the parameters: polydispersity index (PDI), Particle size (PS) and zeta potential (ZP); (**B**) Response surface graphics for preparation methods in cold (**Left**) and hot (**Right**) for the parameters: encapsulation efficiency (EE), aspect ratio (AR) and desirability.

In general, the PDI increased at low FALs. This can be explained by the fluidity of phospholipids, which rendered ethosomes susceptible to ionic interactions when the FAL was high. The PDI was determined using the DLS method where particles passed through a laser beam at an angle that was inversely proportional to their size. This index is a number calculated from a simple two parameter fit to the correlation data (the cumulants analysis). The PDI is dimensionless and scaled such that values smaller than 0.05 are rarely seen except for highly monodisperse standards. Values greater than 0.7 indicate a very broad size distribution and is probably not suitable for the dynamic light scattering (DLS) measurement. Thus, large particles disperse light at low angles, whereas small particles disperse light at high angles. The PDI values of all samples were lower than 0.6, and the samples labeled as 3H and 4H presented the lowest PDI values (<0.25), while also exhibiting relatively narrow size distributions. Figure 2 illustrates that a large HR and low FAL resulted in lower PDI values.

The FAL amounts caused significant differences in the ZP values, and thus, a large FAL (100 mg) caused the ethosomal systems to become less negative. Conversely, ZP increased at low FALs, thus increasing the stability of ethosomes by preventing their fusion and aggregation due to electrostatic repulsions [28]. Therefore, the symmetry of particles decreased when short HT were employed. In fact, it was necessary to consume mechanical energy to produce these ethosomal colloidal systems. In turn, this was eased by the hydration and swelling of the phospholipid bilayers transforming from semi-spherical or ellipsoids into spherical vesicles. The pH values of all ethosomal systems were slightly acidic to neutral and were highly associated with the FAL. Thus, the pH of the samples presenting the largest load (100 mg) ranged from 6.1 to 6.2, whereas the pH value of the samples characterized by low FALs (10 mg) were higher (6.52–6.53), and were comparable to the pH of the FA-free ethosomal systems (6.55). Furthermore, the pH values of all ethosomes were higher than the pKa of FA (4.58), and thus, the ionized form of FA was prevalent, but both the ionized and nonionized forms of FA were expected to be trapped within the vesicles.

3.3. EE Analysis

The EE of the ethosomes was significantly affected by the FAL. As the FAL increased, EE decreased. Furthermore, the presence of ethanol increased the solubility and entrapment of FA within the ethosomal media since the solubility of FA in ethanol (50 mg/mL) is much higher than that in water (0.78 mg/mL). Therefore, the interactions between the internal hydrogen bonds between phosphate or hydroxyl groups could lead to the rapid and compacted binding of FA within the phospholipids and to greater intermolecular spacing within the cores of the ethosomes. Thus, FA could interact with the ethosomes due to the polar and nonpolar forces and/or electrostatic interactions with the phospholipids head groups. The optimization runs were obtained by building surface plots based on the factorial models obtained for each response. In our study, these conditions were satisfied when the ethosomal systems exhibited the most optimal morphology, highest EE, highest ZP, and lowest PDI. None of the other response variables were restricted and remained within the range of the dataset. Thus, the best predicted operational parameters that met the abovementioned conditions produced a desirability of 0.8 while employing a low FAL and high HT, independent of the HR (Figure 2).

3.4. FT-IR and DSC Characterization of the Optimized Ethosomal System

The results of the FT-IR and DSC characterization of the optimized ethosomal system are shown in Figure 3.

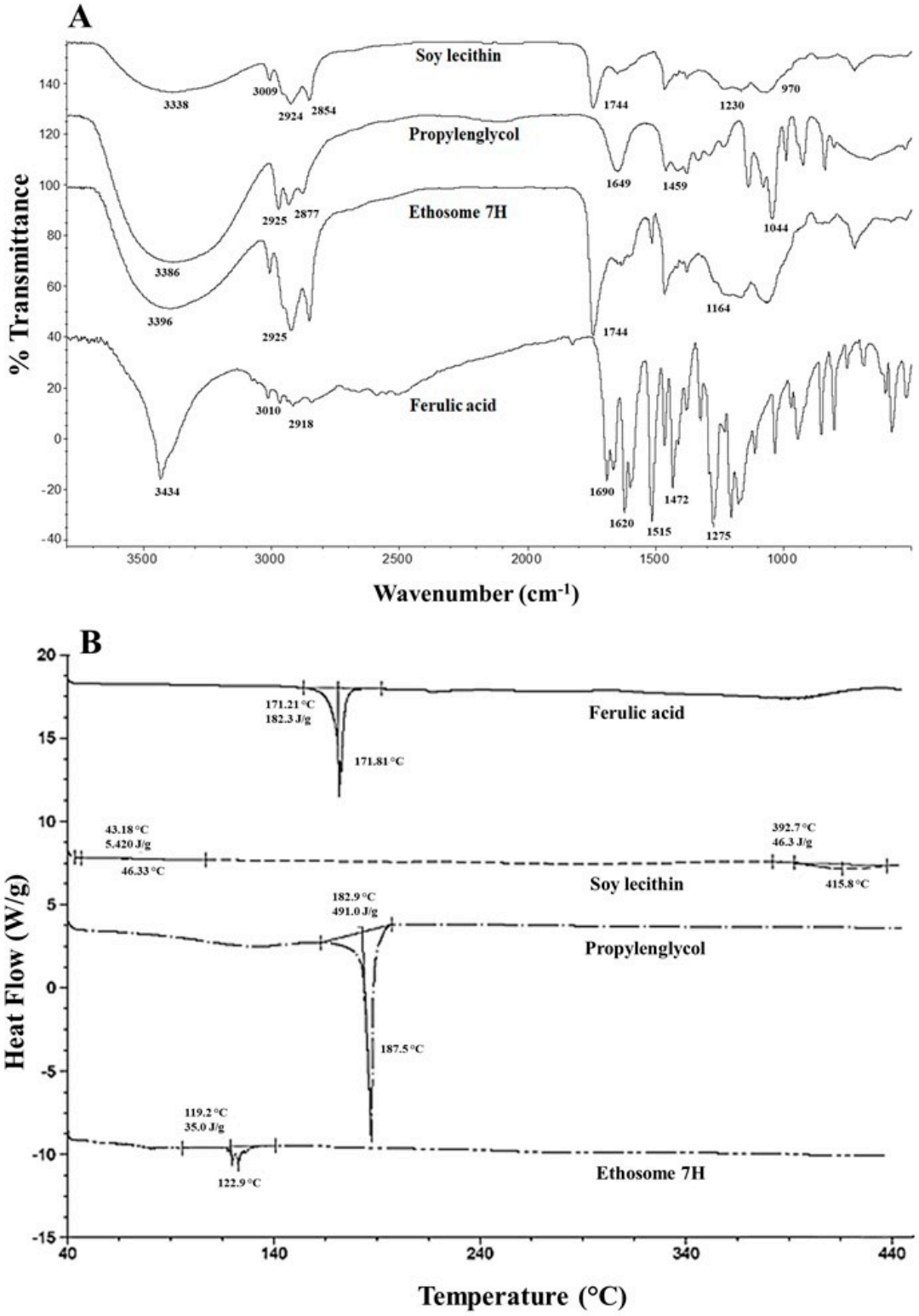

Figure 3. (**A**) FT-IR spectra and (**B**) DSC thermograms of FA, soy lecithin, propylene glycol, and ethosome samples.

The vibrational bands at 3434, 3010, and 2918 cm^{-1} in the FT-IR spectrum of FA were attributed to the stretching of the OH of the carboxyl group, stretching of the C–H of the aromatic ring, and symmetrical and asymmetric stretching of the CH_3 groups, respectively (Figure 3A). Furthermore, the 1690 and 1275 cm^{-1} bands in the FT-IR spectra of FA were attributed to the stretching of the C=O and

C–O–C bonds of the carboxyl group, respectively. In addition, the signals at 1620 and 1515–1432 cm^{-1} were assigned to the stretching of the C=C bonds of the aromatic ring. Moreover, the band at 1665 cm^{-1} was ascribed to the alkene group and the bands between 900 and 650 cm^{-1} were attributed to the CH interactions [24,29]. On the other hand, soy lecithin exhibited a broad band above 3388 cm^{-1} due to the stretching of the OH and amino groups. Other bands at 3009, 2924, and 2854 cm^{-1} were attributed to the symmetrical and asymmetric stretching of the CH_2 and CH_3 groups and to CH_2 scissoring, respectively. Moreover, the signal at 1744 cm^{-1} corresponded to the stretching of the ester bond. Furthermore, the overlapping vibrational bands of the PO^{2-} and P–O–C groups occurred between 1230 and 970 cm^{-1} [30,31]. The signal at 1230 cm^{-1} was due to the formation of hydrogen bonds between the phosphate head groups and the surrounding water molecules [32]. The spectrum of propylene glycol presented vibrational bands at 1044 cm^{-1} due to the stretching of the C–OH bonds, a band at 3386 cm^{-1} due to the stretching of the OH groups, and signals at 2925, 2877, and 1459 cm^{-1} attributed to the symmetrical and asymmetric stretching of the CH_2 and CH_3 groups and scissoring of CH_2, respectively [33]. The band at 1649 cm^{-1} was attributed to the stretching of C=O possibly due to traces of impurities corresponding to an ester group. On the other hand, the aqueous ethosomal dispersion exhibited bands at 3396, 2925, 1744, and 1164 cm^{-1}, which mostly matched the bands observed for soy lecithin, thus indicating its prevalence in the aqueous ethosomal dispersion. It is worth mentioning that soy lecithin accounted for only 3% of the composition of ethosomes as compared to propylene glycol, which accounted for 20% of their composition.

On the other hand, we used DSC analysis to identify thermal events and obtain information on the composition of the ethosomes (Figure 3B). Based on the thermograms, we determined that the melting point and enthalpy of FA were 171.8 °C and 182.3 J/g, respectively. Moreover, FA did not present an amorphous phase or a glass transition, but exhibited an exothermic onset peak due to thermal degradation beyond 397.7 °C. The phase transition temperature of soy lecithin was reported to range between 55 and 65 °C, and in our study occurred at 58.1 °C. In addition, another endothermic change started at approximately 392.1 °C, since soy lecithin is a mixture of phospholipids, such as PC, phosphatidylethanolamine, lysophosphatidylcholine, *N*-acyl-phosphatidylethanolamine, and phosphatidylinositol, and all of them contributed to the phase transition temperature [34]. The thermogram for propylene glycol presented an endothermic peak at 187.47 °C, which was attributed to its boiling point, and the corresponding transition enthalpy was 501.0 J/g. The ethosomal vesicles exhibited an endothermic peak at 187.5 °C and an enthalpy of 435.7 J/g due to the interdigitation of their chains, which indicated that they presented a crystalline, regular structure and homogeneous heat flux. For comparison, the endothermic peak of the phospholipids in soy lecithin was observed at 416.8 °C. These results were in agreement with those reported in the literature for other vesicles, where the inclusion of soy lecithin caused hydrophobic interactions in the vesicle bilayer, thus resulting in a less rigid lipid bilayer which eased the permeability and decreased the melting point of the ethosomes. In addition, the signal and enthalpy of FA in the ethosomal system also decreased, shifting toward 122.9 °C and 30.8 J/g, respectively, therefore indicating a lower degree of crystallinity or higher amorphicity.

3.5. DLS Characterization of Optimized Ethosomal Systems

The effect of pH on the optimized ethosomal dispersion is depicted in Figure 4. The ZP value became more electronegative (−54.8 mV at pH 5.4) as the pH of the media approached neutrality (Figure 4A). This was essentially attributed to the ionization of phospholipids containing soy lecithin and incorporated FA, which generated negative charges on the phosphate groups located on the surfaces of the vesicles. The interaction between phospholipids and FA is known to be specific and dependent on polar and van der Waals interactions. Van der Waals interactions occur between the hydrocarbon chains and aromatic rings and between the polar heads of phospholipids and carboxyl groups leading to compact and rapid binding of FA, which results in increased intermolecular spaces between the polar heads. On the other hand, the size of the ethosomal vesicles did not present any

trend as the pH changed. Vesicle size presented minimum and maximum values of 453 and 598 nm at pH 2.2 and 3.8, respectively. In addition, ZP reached a plateau at ~4.5 probably due to the contribution of FA since its pKa is 4.5 and, at this pH, equal contributions of the ionized and nonionized forms of FA were expected. The lower the pH or acidity of the media the higher the availability of H^+ ions to create a shielding charge on the surface of the ethosomes, which led to a less negative charge (–55 to –40 mV). However, at higher pH levels, the ionized form of FA was prevalent and contributed to the negative value of the surface charge of the vesicles. On the other hand, the particle size of the vesicles reached a maximum when the pH ranged between 3.8 and 4.5, possibly due to the interaction of the hydrophilic heads of the phospholipids with FA causing a displacement of the acid-base equilibrium. Furthermore, the pKa of PC was ~4, and thus, at this pH the size variation or compaction of ethosomes was large and hence, a singularity was observed in the PDI (Figure 4B).

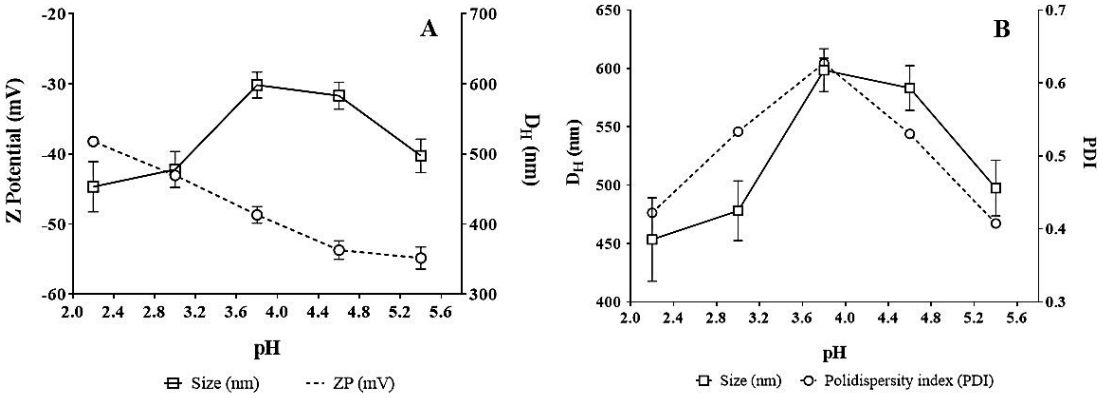

Figure 4. Effect of pH on: (**A**) zeta potential and (**B**) particle size (D_H: Hydrodynamic Diameter) of optimized ethosomal system.

3.6. Performance Tests of the Optimized Ethosomal System

In-Vitro Permeability Test

It is widely accepted that ethosomal systems increase the permeation of solutes through the skin [21]. The enhanced absorption of solutes is attributed to ethanol, which penetrates the intercellular membrane lipids, decreasing their density and increasing their fluidity. Furthermore, ethanol evaporates rapidly at skin temperature (~32 °C) and alters the solubility properties of stratum corneum, thus easing the partitioning of the solute. The in-vitro diffusion permeability of FA from different ethosomal formulations was studied using Franz cells. The effective permeation area of the cell and volume of the receptor cell were 0.79 cm^2 and 13 mL, respectively. First, the same medium used to prepare the ethosomal systems was used (solution A). For this test, an uncoated cellulose membrane was used to determine the permeability properties of FA and find a membrane featuring characteristics similar to those of the commercial one (Strat-M®). Subsequently, the cellulose membrane was coated with a thin layer of soy lecithin, and a pH 7.4 buffer (solution B), was used in the receptor medium. This buffer was chosen because its pH was like the pH of skin. Tests were carried out using the Strat-M® membrane, and the permeability of the free and encapsulated FA was evaluated. Aliquots of 1.0 mL each were collected through the sampling port of the cell at 1, 2, 3, 4, 5, and 6 hours. The surface area of FA is high (66.8 $Å^2$), moreover, FA can generate an anionic charge on the carboxyl group and presents remarkable hydrophobicity due to its phenyl moiety. In addition, the aqueous solubility (0.78 mg/L) and permeability (logP = 1.51) of FA are low, therefore FA is a Class II substance according to the Biopharmaceutical Classification System [5]. Figure 5 and Table 2 present the permeability profiles and parameters of FA in different media and at different pH levels, respectively. The phospholipid membrane of molecules of small molecular weight which present moderate aqueous solubility, such as FA, constitutes a very faint barrier. Since the molecular weight of FA is only 194.2 g/mol, which is

significantly lower than 1000 g/mol, it is expected that FA would pass easily through the membrane pores. Furthermore, its high ethanol content causes a less tightly packed structure of the ethosomal membrane compared to that of conventional liposomal vesicles. This would grant the ethosomal membrane a smoother and more flexible structure, rendering more freedom and stability to the membrane and easing the formation of pores for the release of FA [35].

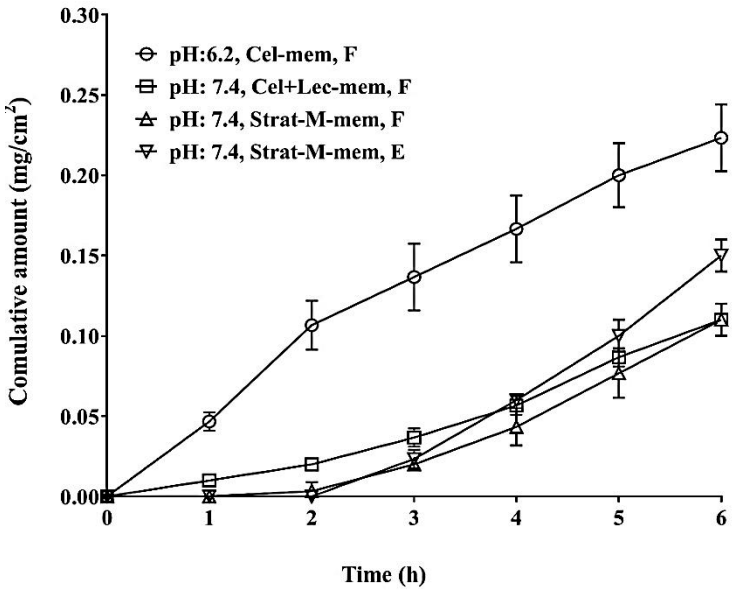

Figure 5. Membrane diffusion studies of FA. Cel-mem: Cellulose membrane, Cel+lec-mem: Cellulose membrane with soy lecithin, Strat-M-mem: Strat-M® membrane, F: free compound, and E: encapsulated compound.

Table 2. Permeability parameters.

Parameter	pH 6.2 Cel-mem, F	pH 7.4 Cel-mem, F	pH 7.4 Strat-M-mem, F	pH 7.4 Strat-M-mem, E
Diffusion Coefficient D (cm^2/s)	0.068	0.034	0.037	0.044
Lag Time (h)	0	0.76	1.94	1.96
Flux ($mg \cdot h/cm^2$)	0.77	0.28	0.27	0.35

Cel-mem: Cellulose membrane, Strat-M-mem: Strat-M® membrane, F: free compound, and E: encapsulated compound.

It is believed that FA was mostly entrapped within the hydrophilic core of the ethosomes, and thus was released from the ethosomes by passive diffusion driven by the concentration gradient across the vesicular lipid bilayer. Furthermore, the chemical composition of the membrane significantly altered the in-vitro release of FA. Other factors such as the pH of the medium and surface porosity could also be responsible for the initial lag time and slow release of FA from the ethosomes. Therefore, the cellulose membrane featuring pore diameters of 0.45 µm and a soy lecithin coating presented the highest permeability compared with other membranes. However, as the pH increased from 6.2 to 7.4, permeability (indicated by the Flux) was reduced from 0.77 to 0.28 $mg \cdot h/cm^2$. On the other hand, the Strat-M® membrane which simulated the dermal permeability demonstrated that the permeability of the encapsulated product was greater than that of the product containing free FA (0.34 and 0.26 $mg \cdot h/cm^2$, respectively). The Strat-M® membrane is a synthetic membrane-based model, and its diffusion characteristics correlate well to those of human skin [36]. These results were corroborated by the amount of FA released after 6 h and the values of the diffusion coefficient. Thus, the product containing free FA released ~4.8% of the total FA, whereas the optimal dispersion of ethosomes indicated 7.1% permeation. The values of the diffusion coefficient (0.044 vs. 0.037 cm^2/s)

were determined by adjusting the experimental values to a specific error function model at a release distance of 1 cm. At pH 7.4, the behavior of the cellulose membrane moistened with soy lecithin was comparable to that of the Strat-M® membrane. This could allow for large-scale trials for these vesicles, which would be more affordable than the Strat-M® membrane. Furthermore, the release profile of FA from the Strat-M® membranes was biphasic, and presented an initial lag time of ~2 h, whereas the initial lag times of the cellulose membranes tested at pH 6.2 and 7.4 were 0 and 0.8 h, respectively. Once the lag time was surpassed a steep release period followed for all tested membranes, which presented an almost linear profile.

4. Conclusions

This study presented a rapid method for preparing ethosomal colloidal systems which involved no harmful solvents or detergents. The prepared vesicles exhibited good stability, size distribution, and morphology, and mainly consisted of LUV, MLV, and OLV. The ZP values of the formulations were in the negative range and exhibited slight decreases in different factors as charge intensity upon the inclusion of FA, hydration conditions, and hydration temperature. Furthermore, the ethosomal systems may improve the permeability of FA, thus representing a promising alternative for the topical administration of antioxidants, which are used to reduce the oxidative damage to the skin caused by solar radiation.

Author Contributions: C.A.L. prepared and characterized the ethosomal systems, C.J.Y. made the characterization in aqueous media and the permeability assay, whereas J.R. and C.H.S. advised the work, analyzed the data and wrote the manuscript.

Funding: This research received no external funding.

Acknowledgments: The authors are grateful to the committee for the development of research (CODI) of the University of Antioquia its Sustainability Strategy Program (2018-2019) for their financial support. The authors would like to especially thank Icesi University for the internal grant CA041368.

Conflicts of Interest: The authors declare no commercial interest that could represent a conflict related to this study.

References

1. World Health Organization. Skin Cancers. Available online: https://www.who.int/uv/faq/skincancer/en/index1.html (accessed on 18 January 2018).
2. Rojas, J.; Londoño, C.; Ciro, Y. The health benefits of natural skin UVA photoprotective compounds found in botanical sources. *Int. J. Pharm. Pharm. Sci.* **2016**, *8*, 13–23.
3. Harwansh, R.K.; Mukherjee, P.K.; Bahadur, S.; Biswas, R. Enhanced permeability of ferulic acid loaded nanoemulsion based gel through skin against UVA mediated oxidative stress. *Life Sci.* **2015**, *141*, 202–211. [CrossRef] [PubMed]
4. Chang, M.; Chang, C. Determination of four lipophilic phenolics in o/w emulsions as well as their stability. *Chia-Nan Annu. Bull.* **2012**, *38*, 91–101.
5. Ingredients Ferulic Acid. Available online: https://www.ewg.org/skindeep/ingredient/702470/FERULIC_ACID/ (accessed on 18 January 2018).
6. Zhu, H.; Liang, Q.; Xiong, X.; Chen, J.; Wu, D.; Wang, Y.; Yang, B.; Zhang, Y.; Huang, X. Anti-Inflammatory Effects of the Bioactive Compound Ferulic Acid Contained in *Oldenlandia diffusa* on Collagen-Induced Arthritis in Rats. *eCAM* **2014**, *2014*, 573801. [PubMed]
7. Rakesh, R.; Anoop, K. Ethosomes for transdermal and topical drug delivery. *Int. J. Pharm. Pharm. Sci.* **2012**, *4*, 17–24.
8. Verma, P.; Pathak, K. Therapeutic and cosmeceutical potential of ethosomes: An overview. *J. Adv. Pharm. Technol. Res.* **2010**, *1*, 274–282. [CrossRef] [PubMed]
9. Manca, M.; Castangia, I.; Matricardi, P.; Lampis, S.; Busquets, X.; Fadda, A.; Manconi, M. Molecular Arrangements and Interconnected Bilayer Formation Induced by Alcohol or Polyalcohol in Phospholipid Vesicles. *Colloids Surf. B Biointerfaces* **2014**, *117*, 360–367. [CrossRef] [PubMed]

10. Grit, M.; De Srnidt, J.H.; Struijke, A.; Crommelin, D. Hydrolysis of phosphatidylcholine in aqueous liposome dispersions. *Int. J. Pharm.* **1989**, *50*, 1–6. [CrossRef]
11. Brandl, M. Liposomes as drug carriers: A technological approach. *Biotechnol. Annu. Rev.* **2001**, *7*, 59–85. [PubMed]
12. Blume, G.; Cevc, G. Molecular mechanism of the lipid vesicle longevity in vivo. *BBA Biomembr.* **1993**, *1146*, 157–168. [CrossRef]
13. Kanehisa, M.; Tsong, T. Cluster model of lipid phase transitions with application to passive permeation of molecules and structure relaxations in lipid bilayers. *J. Am. Chem. Soc.* **1978**, *100*, 424–432. [CrossRef]
14. Lodzki, M.; Godin, B.; Rakou, L.; Mechoulam, R.; Gallily, R.; Touitou, E. Cannabidiol—Transdermal delivery and anti-inflammatory effect in a murine model. *J. Control. Release* **2003**, *93*, 377–387. [CrossRef] [PubMed]
15. Panwar, R.; Pemmaraju, S.C.; Sharma, A.K.; Pruthi, V. Efficacy of ferulic acid encapsulated chitosan nanoparticles against *Candida albicans* biofilm. *Microb. Pathog.* **2016**, *95*, 21–31. [CrossRef] [PubMed]
16. Castangia, I.; Manca, M.; Matricardi, P.; Sinico, C.; Lampis, S.; Busquets, X.; Fadda, A.; Manconi, M. Effect of Diclofenac and Glycol Intercalation on Structural Assembly of Phospholipid Lamellar Vesicles. *Int. J. Pharm.* **2013**, *456*, 1–9. [CrossRef] [PubMed]
17. Lian, T.; Ho, R. Trends and Developments in Liposome Drug Delivery Systems. *J. Pharm. Sci.* **2001**, *90*, 667–680. [CrossRef]
18. Bhalaria, M.; Naik, S.; Misra, A. Ethosomes: A novel delivery system for antifungal drugs in the treatment of topical fungal diseases. *Indian J. Exp. Biol.* **2009**, *47*, 368–375. [PubMed]
19. Uchida, T.; Kadhum, W.; Kanai, S.; Oshizaka, T.; Todo, H.; Sugibayashi, K. Prediction of skin permeation by chemical compounds using the artificial membrane, Strat-M^{TM}. *Eur. J. Pharm. Sci.* **2015**, *67*, 113–118. [CrossRef] [PubMed]
20. Simon, A.; Amaro, M.; Healy, A.; Cabral, L.; de Sousa, V. Comparative evaluation of rivastigmine permeation from a transdermal system in the Franz cell using synthetic membranes and pig ear skin with in vivo-in vitro correlation. *Int. J. Pharm.* **2016**, *512*, 234–241. [CrossRef]
21. Touitou, E.; Dayan, N.; Bergelson, L.; Godin, B.; Eliaz, M. Ethosomes—Novel vesicular carriers for enhanced delivery: Characterization and skin penetration properties. *J. Control. Release* **2000**, *65*, 403–418. [CrossRef]
22. Chapman, D.; Arrondo, J. Recent studies of liposomes and modifications of their structures. In *Liposomes Drugs and Immunocompetent Cell Function*; Nicolau, C., Paraf, A., Eds.; Academic Press: London, UK, 1981.
23. Weiner, A.; Carpenter-Green, S.; Soehngen, E.; Lenk, R.; Popescu, M. Liposome–Collagen Gel Matrix: A Novel Sustained Drug Delivery System. *J. Pharm. Sci.* **1985**, *74*, 922–925. [CrossRef] [PubMed]
24. Lee, D.; Chapman, D. Infrared Spectroscopic Studies of Biomembranes and Model Membranes. *Biosci. Rep.* **1986**, *6*, 235–256. [CrossRef] [PubMed]
25. Maurer, N.; Fenske, D.; Cullis, P. Developments in liposomal drug delivery systems. *Expert Opin. Biol. Ther.* **2001**, *1*, 923–947. [CrossRef]
26. Malekar, S. Liposomes for the Controlled Delivery of Multiple Drugs. Ph.D. Thesis, University of Rhode Island, Kingston, RI, USA, 2014.
27. Bergstrand, N. Liposomes for Drug Delivery: From Physico-Chemical Studies to Applications. Ph.D. Thesis, Acta Universitatis Upsaliensis, Uppsala, Sweden, 2003.
28. Kan, P.; Tsao, C.; Wang, A.; Su, W.; Liang, H. A liposomal formulation able to incorporate a high content of Paclitaxel and exert promising anticancer effect. *J. Drug Deliv.* **2011**, *2011*, 629234. [CrossRef]
29. Torres, J.; Durás, S. Fosfolípidos: Propiedades y efectos sobre la salud. *Nutr. Hosp.* **2015**, *31*, 76–83.
30. Kuligowski, J.; Quintás, G.; Garrigues, S.; De la Guardia, M. Determination of lecithin and soybean oil in dietary supplements using partial least squares–Fourier transform infrared spectroscopy. *Talanta* **2008**, *77*, 229–234. [CrossRef] [PubMed]
31. Choudhary, N.; Pardhi, D.; Bhoyar, M. Isolation of soy lecithin from soy sludge, its standardization and behavioural stud. *Asian J. Pharm. Clin. Res.* **2013**, *6*, 133–136.
32. Ingvarsson, P.; Yang, M.; Nielsen, H. Stabilization of liposomes during drying. *Expert Opin. Drug Deliv.* **2011**, *8*, 375–388. [CrossRef] [PubMed]
33. Shinzawa, H.; Uchimaru, T.; Mizukado, J.; Kazarian, S.G. Non-equilibrium behavior of polyethylene glycol (PEG)/polypropylene glycol (PPG) mixture studied by Fourier transform infrared (FTIR) spectroscopy. *Vib. Spectrosc.* **2017**, *88*, 49–55. [CrossRef]

34. Exton, J. Phosphatidylcholine breakdown and signal transduction. *Biochim. Biophys. Acta* **1994**, *1212*, 26–42. [CrossRef]
35. Kashchiev, D.; Exerowa, D. Bilayer lipid membrane permeation and rupture due to hole formation. *Biochim. Biophys. Acta* **1983**, *732*, 133–145. [CrossRef]
36. DeCoste, J. Study Finds Merck Millipore's Strat-M®Synthetic Membrane Comparable to Human and Animal Skin for Permeation Studies. Available online: https://www.merckgroup.com/content/dam/web/corporate/non-images/press-releases/2015/may/en/Strat-M-EN.pdf (accessed on 18 January 2018).